TESTING LONG-WAVELENGTH ACOUSTIC FLOWMETER CONCEPTS FOR FLUE GAS FLOWS

Lee J. Gorny[1], Keith A. Gillis[2], and Michael R. Moldover[2]

[1] *Department of Mechanical Engineering, The University of Maryland, College Park, MD 20742*

[2] *Sensor Science Division, National Institute of Standards and Technology, Gaithersburg, MD 20899*

As a part of NIST's program to standardize measurements of greenhouse gas emissions, we are developing a long-wavelength acoustic flowmeter (LWAF) for accurate, economical measurements of exhaust flows from coal-burning power plants. Measurements of the flue gas mass flow combined with the gas's composition are used to determine the emitted CO_2 and other by-products of combustion. Today, such measurements have uncertainties of 5 % or more due to the large size of the flue-gas stacks and the flow's non-uniform, unsteady, and swirling profile. A LWAF averages the spatial non-uniformities of the axial velocity over the entire cross section in a manner insensitive to flow distortions. In contrast, conventional techniques measure gas flow only at isolated points or averaged along chords across the stack. We constructed a 1:100 scale, calibrated flow facility for the initial development of a LWAF. In preliminary tests of three flow metering methods, uncertainties ranged from 1.4 % to 4.9 %, compared to our target uncertainty of 1 %. We present the principle behind the LWAF, our design considerations, and the current performance of time and frequency-based approaches to metering, and describe technical challenges that must be overcome to use a LWAF at a full-scale power plant.

1. Introduction

We are developing a long-wavelength acoustic flowmeter (LWAF) to accurately and economically measure power plant exhaust flows. Such a device could replace current flow-measurement methods, improve flow determinations in process monitoring and optimization, and provide plants with a continuous emissions monitoring system (CEMS) having a reduced measurement uncertainty. Accurate measurement of mass flow, combined with assessment of the gas's composition allows for quantification of CO_2 and other emissions. Development and commercialization of advanced technologies enhances the accuracy of the greenhouse gas inventory determinations and improves regulatory efforts nationally and worldwide. Under current state and federal regulations, a substantial cost savings to energy providers would be realized if an inherently accurate method with sufficient sensitivity were used, obviating the need for frequent costly calibrations. If future regulations or taxes are based on emission, the financial incentives for accurate flue gas measurements will increase greatly.

Due to the large scale, non-uniform, unsteady, and swirling flow profile of exhaust gas, current flowmeters have significant measurement uncertainties that are difficult to quantify over the full range of plant operational profiles. Potzick and Robertson first investigated LWAF techniques at the National Bureau of Standards (NBS) in the mid 1970's [1, 2, 3]. In its simplest embodiment, a LWAF determines flow from measurements of the propagation characteristics of acoustic plane waves in a duct or pipe. This early metering approach was effective in complex, unsteady flows having a Mach number (Ma = flow velocity/speed of sound in the fluid medium) < 0.1 [3]. As shown in [1], flow distortions change the propagation of plane waves in proportion to Ma^2 in a first approximation (Flue gas flows from coal-burning power plants have $Ma < 0.058$ [6]). High

levels of blower-induced and turbulence-generated noise (which scales as Reynolds Number $(Re)^8$ [4]), exist in the range $10^6 < Re < 10^8$ inside large flue gas stacks making it difficult to scale up Potzick and Robertson's approach. However, technological advancements in signal processing, flow modeling, and sensor technology stimulated us to re-examine long wave acoustic methods with the hope that a robust flow-measurement method will result.

We describe measurements taken during the first of a three-phase testing strategy to develop and validate new LWAF flow measurement approaches. We built a 1:100 scale (0.1 m diameter) flow facility (described in detail in Section 2 of this paper) to test alternative LWAF concepts. Successful concepts will be verified in either the 1 m-diameter flow calibration facility currently being assembled by the National Institute of Standards and Technology's (NIST) Fluid Metrology Group or in NIST's National Fire Resistance Lab's (NFRL's) ~1.5 m exhaust stack. These larger facilities will screen measurement concepts for scale-up to a full-size stack.

During summer 2011, we measured the flow noise and vibration levels in a flue gas exhaust stack of a 555 MW coal-burning, power plant. We found two tones 1.8 Hz and 2.3 Hz of sufficiently low frequency to drive a LWAF. Except for these tones, the pressure-fluctuation-spectrum measured was broadband and incoherent at low frequencies, as expected from turbulent flow in the stack. Tones were present at frequencies above 750 Hz, but unfortunately these are well above the duct cut-on frequency (f_{co}) (*i.e.* the frequency above where pressure waves can propagate non-axially along the duct as higher order modes); therefore, these tones were unsuitable for driving a LWAF.

In this paper, we test frequency- (*f*) and time- (*t*) domain based LWAF measurement concepts using our calibrated, 1:100 scale, flow facility at velocities up to 5 m/s (0.047 kg/s). The LWAF measured flows with uncertainties ranging from 1.4 % to 4.9 % in distorted swirling flow (Unless otherwise specified, uncertainties reported are standard uncertainties corresponding to a 68 % confidence level). We present an overview of the test facility in Section 2, discuss *f* and *t* based methods in Sections 3 and 4 respectively and present our conclusions in Section 5.

2. 1:100 Scale LWAF

To set the context for our model test facility, we briefly describe the flow of flue gases in the stack of a large coal-burning power plant. Then we describe the mechanical construction of the LWAF test facility and finally, the instrumentation that we use to acquire and analyze test data.

2a. Context for the test facility

In a commercial power plants, the inner diameter of the flue-gas stack ranges up to 37 m. Typically, the largest diameters are found in older, higher capacity plants, or those requiring greater dispersion to meet regulatory requirements. In modern plants, lined stacks are increasingly used. These two-part stacks have a concrete structural stack (visible from the outside) that houses one or several smaller liners that serve as the flue. When compared to brick or concrete stacks, stack liners made of fiberglass reinforced polymer provide enhanced corrosion resistance and enable higher velocity flow because of their reduced surface roughness. Power plants, regardless of their size, have typical liner diameters that are 10 m or less [5].

The Electric Power Research Institute (EPRI) recommends stack velocities on the order of 15 m/s to 18 m/s for a wet stack (where a scrubber saturates the exhaust gas) with a typical liner in a coal-fired plant. Maximum flow speeds can be as high as 20 m/s for borosilicate glass liners and as low as 12 m/s for brick lined concrete stacks. By comparison, natural gas turbines typically use smaller ducts with flows as high as 40 m/s [6]. Reynolds numbers for coal plant flue gas range from 5×10^6 to 3×10^7. The cut-on frequency (f_{co}) of a 10 m diameter duct is 20 Hz, which is the lower threshold of human hearing. The relevant parameters are defined as

$$Re = \rho V D / \mu \tag{1}$$

$$f_{co} = 1.841 c / (\pi D) \tag{2}$$

$$c = (\rho \kappa_s)^{-1/2} \tag{3}$$

where ρ is the density of the fluid medium, μ is the dynamic (shear) viscosity, V is the linear flow velocity, D is the diameter of the duct, c is the speed of sound, κ_s is the adiabatic compressibility of the fluid.

2b.   Test Facility

We built the 1:100 scale flow testing facility shown in Fig. 1. The facility has four sections: 1) an inlet section that provides uniform, un-distorted flow into the facility, 2) a reference section containing a calibrated flow meter that measures the uniform flow with a relative uncertainty of 0.2 %, 3) an out-of-plane return bend that generates swirl, and 4) the LWAF test section. The LWAF test section contains a loudspeaker array, a microphone array, and an-easily modified outlet. The joints in the test facility were milled or turned flush and smoothed to minimize unintentional flow distortion, flow-generated sound, and energy loss.
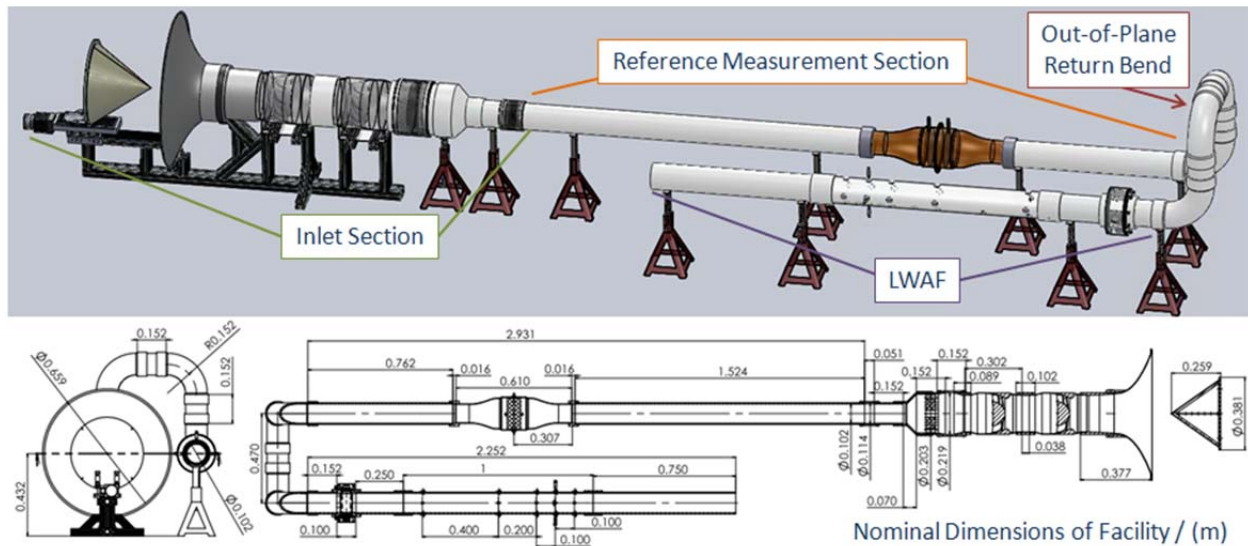

Figure 1: Diagram of the 1:100 scale LWAF testing facility with nominal dimensions.

Our goal is to be capable of obtaining a maximum velocity of 32 m/s with this facility. This number is well above the maximum flows in coal plant stacks and is approximately $Ma = 0.1$. Above $Ma = 0.1$, poorly-understood corrections of order Ma^2 need to be added to the LWAF model, which reduce its accuracy. Velocity scaling was impractical in our model facility; however, turbulence, Re considerations and considerations of the noise floor measured in a stack will be addressed in later work. In the laboratory, and in the test cases presented in Sections 3 and 4 of this paper, we use two small fans (shown in Fig. 2), which generate flows up to 5 m/s. This relatively low velocity is due to the insertion loss of our laminar flow meter (LFM). In future work, we will test flowmeter concepts discussed up to 30 m/s using a larger 3.73 kW (5 HP) centrifugal blower.
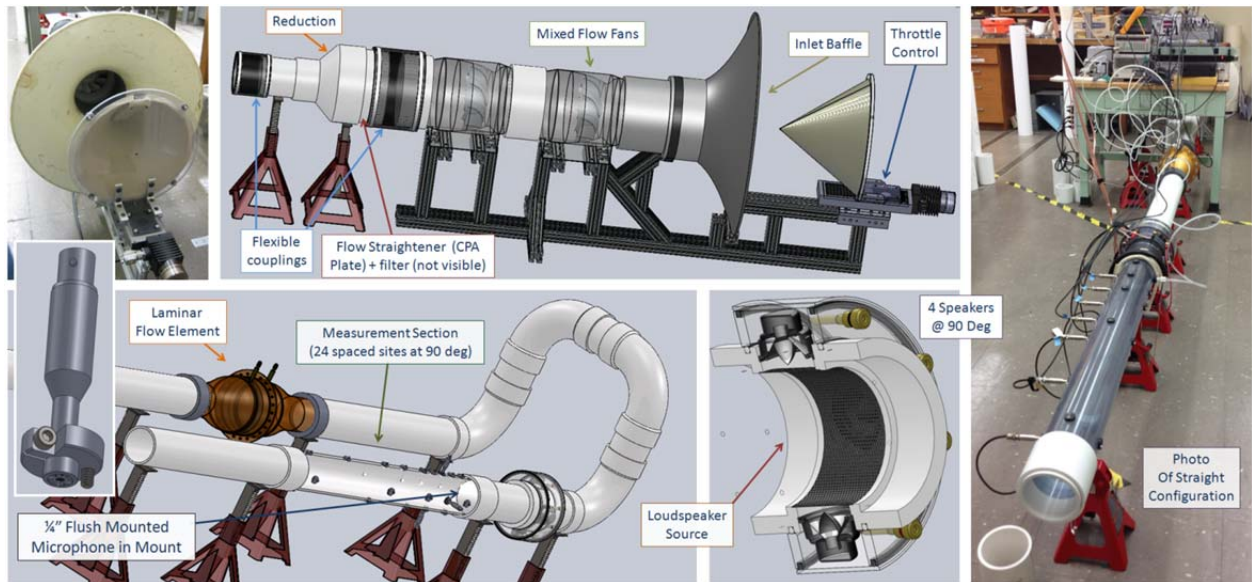

Figure 2: Detail views of inlet and LWAF sections of 1/100 scale facility.

Both the reference and LWAF measurement sections were constructed primarily of 0.102 m (4 inch) diameter, schedule 40, polyvinyl chloride (PVC) pipe. In order to ensure that a fully developed, undistorted flow enters the LFM, 15 and 7.5 diameters of straight pipe were placed upstream and downstream, respectively. These sections allow flow distortions from the upstream fans to settle and isolate the flowmeter from swirl in the downstream flow generated by the 2-axis turnaround. The facility's outlet abruptly terminates, to acoustically emulate the exit of the duct liner of a power plant. The abrupt termination strongly reflects sound waves due to the abrupt impedance change between the inside of the duct and the open ambient environment.

A key design aspect of the 1:100 scale facility is its modularity. If changes need to be made, these are straightforward. For example, the two-axis bend shown in Fig. 1 can be removed by attaching the LWAF section directly downstream of the reference section as shown in the picture on the right of Fig. 2. The microphone array can be moved relative to the loudspeaker and facility's open end simply by changing the upstream and downstream PVC sections. Furthermore, the facility can be converted to operate as a closed loop by removing the inlet bell mouth and throttle upstream of the fans, and then adding a second 90 degree bend with additional larger diameter pipe length beyond the outlet. Other additions in the future will likely

include a heat exchanger to add or remove heat as necessary, a means for humidification, and a turbulence generator to better emulate the flow inside of a stack. Flow visualization along with multiple axis hot-wire anemometry will be used in the clear measurement section to characterize flow profiles and assess their impact on LWAF measurement.

The test facility's inlet section is shown in the top left of Fig. 2. Components were mounted on 80/20 brand aluminum framing for structural support. Two inline Solar and Palau (S+P) [8] model TD-200 mixed flow fans generate the flow. Air is drawn in through a tapered baffle made from a trimmed fiberglass sousaphone bell. This inlet is coupled with a cone shaped sound absorbing plug made using perforated sheet metal and acoustic felt to reduce the sound reflected from this end of the facility. The cone throttles flow through the facility and is actuated using a motorized stage driven via GPIB. When the cone rested directly against the baffle, the throttle was "fully closed." The linear motor has a range of 15 cm, and to obtain maximum flow, the motor and cone were retracted 25 cm further along a slider below the motor stage to the "fully opened" position. Each fan has "high" and "low" settings. Using throttling and motor settings, we achieved the nominal flows listed in Table 1.

Table 1: Flow settings used in experimental LWAF evaluations in Sections 3 and 4.

Flow Case for Frequency Based LWAF	Flow Case for Time Based LWAF	Fan Motor 1	Fan Motor 2	Throttle Position	Flow Velocity / (m/s) (Nominal LFM)
1	1	Hi	off	Fully Closed	1.37
2		off	Lo	Fully Closed	1.79
7	2	Hi	off	In -.1 m	2.28
5		Hi	off	In -.15 m	2.8
3	3	Hi	Hi	Fully Closed	3.41
8		Hi	Lo	In -.05 m	3.91
6	4	Hi	Lo	In -.15 m	4.47
4	5	Hi	Hi	Fully Opened	4.95

The reduction section of the inlet serves several functions: (1) it reduces the nominal 0.203 m (8 inch) diameter to 0.102 m (4 inch) diameter schedule 40 PVC; (2) it mitigates swirl and flow distortions using a 0.203 m Canadian Pipelines Accessories (CPA) straightener plate; (3) it houses a filter that retains coarse particles that could contaminate the LFM. (The CPA plate and filter were installed in the larger section to reduce insertion loss from their inclusion.) (4) it isolates blower-generated-vibrations from the measurement section using two flexible couplings placed on either side of the reduction section and with 13 mm thick felt placed between the PVC pipe and supporting jack stands, as shown in Figs. 1 and 2.

A two-axis bend is used in the turnaround section of the facility, as shown in Figs. 1 and 2 to introduce swirl into the flow entering into the LWAF measurement section. Although this flow will have a different profile from what occurs due to the T-shaped inlet of an actual stack's liner, it does give an indication of how effective the LWAF is in a distorted flow.

Downstream, the measurement section of the LWAF consists of 24 mounting holes. Nine are staggered axially in sets of five at (0.05, 0.10 and 0.20) m intervals along a primary face of a clear PVC pipe. On three circumferentially adjacent sides at 90 degrees, five holes are staggered axially in sets of three, with (0.1, 0.2 and 0.4) m spacing. Through these holes, microphones and

other sensors can be placed using spacers such as the one shown holding the microphone at the left of Fig. 2.

2c.   Instrumentation

We used a LabView data acquisition program to communicate with the instruments. This program interfaces with an 8 module cDAQ-9178 compact data acquisition chassis (cDAQ). Two NI-9234 [8] analog input (AI) modules are used to measure the acoustic signals measured by the LWAF at a 51.2 kHz sampling rate, and these provide 2 mA of supply current to the microphone preamps directly. The NI-9234 measures a range of ±5 V with 24-bit resolution. A NI-9263 analog output (AO) sends driving signals to the LWAF. The software generated noise functions, single tone waveforms, sine sweeps, multi-tone sine waves, pulses and arbitrary functions defined by an equation. The LabView software can control additional measurement devices using IEEE 488 communication with a National Instruments GPIB-USB-HS adaptor or RS232/485 serial connection via a 4-port USB to serial adaptor. The data acquired was post-processed using Matlab and Excel. Ultimately, we will complete an algorithm entirely within LabView environment to monitor flow in real time.

A Meriam Process Technologies Z50MC2-4 LFM was used to provide a reference flow having a 0.2 % standard uncertainty over the range of 1.2 m/s to 32 m/s. This level of uncertainty was established using the NIST air flow facility to calibrate the meter relative to a combination of 11 critical flow Venturi (CFV) working standards (each calibrated to 0.025 % $k = 2$ uncertainty on the NIST 677 L *PVTt* primary flow standard [7]). Differential pressure is measured across the LFM using a Yokogawa MT-210 Digital Manometer with a 1 kPa range. A Vaisala PTB 330 barometer is used to measure pressure (*P*) on the low *P* side of the LFM. Pressure on the high *P* side is obtained by summing this measurement with the differential pressure. Temperature *T* is measured by thermistors at three points within the facility; on the high and low pressure sides of the LFM (0.315 m from its center plane), and in the LWAF section. Ambient *T* is measured above the LFM. Each thermistor is read using a Fluke CHUB E-4. Humidity is monitored using a Vaisala HMI 41 handheld meter with a HMP 45 tethered probe placed near the facility's exit.

A Paro Scientific Model 745 barometer measures the static pressure in the LWAF. Four, Tang Band W2-803SM 51 mm (2 inch) full-range loudspeakers (LS) are evenly spaced in an array about the duct's circumference. The arrangement of these speakers ensures that a plane wave is driven when desired and offers the potential to drive higher order modal propagations within the duct. A JBL Model 6215 Power Amplifier with 35 W per channel is used to drive these with signal generated by the Labview cDAQ system.

In the experiments conducted for this paper, a series of 7 PCB 130E20, 6.3 mm (1/4 inch), free-field electret condenser microphones with a bandwidth of 20 Hz to 10 kHz are used with positions as shown in Table 2. Each microphone is calibrated at room temperature across a frequency range of 0 kHz to 5 kHz relative to microphone 1 using a G.R.A.S Sound & Vibration Type 51AB Sound Intensity Calibrator that provides a like response at each microphone to within .1 dB during calibration.

Table 2: Microphone Locations in LWAF section

Mic. Channel	Serial No.	Location (m) (re. Mic 1)	Location (m) (re. LS)	Location (m) (re. Open end)
1	30791	0	0.27	1.15
2	30788	0.1	0.37	1.05
3	30790	0.2	0.47	0.95
4	30789	0.3	0.57	0.85
5	33734	0.4	0.67	0.75
6	33733	0.6	0.87	0.55
7	33735	0.8	1.07	0.35

3. Flow Measurement in the Frequency Domain

We tested two frequency based concepts for measuring flow velocity that build on the work of Potzick and Robertson [1, 2, 3]. Each concept uses broadband frequency information to provide measure the speed of sound in the fluid c and its average flow velocity V. Temporal averaging of the frequency response function (FRF) mitigates random pressure fluctuations from turbulence. Figure 3a shows the LWAF configuration used in this paper, the relative locations of the loudspeaker array, pressure and temperature sensors, and each of 7 microphones used to acquire data. Figure 3b shows the amplitude,   and phase change ϕ_{meas} of two specific standing wave patterns (denoted by 1 and 2).   Standing wave patterns emerge from continuous (or semi-continuous using a swept sine function) driving of acoustic waves between the loudspeaker and open end of the duct.
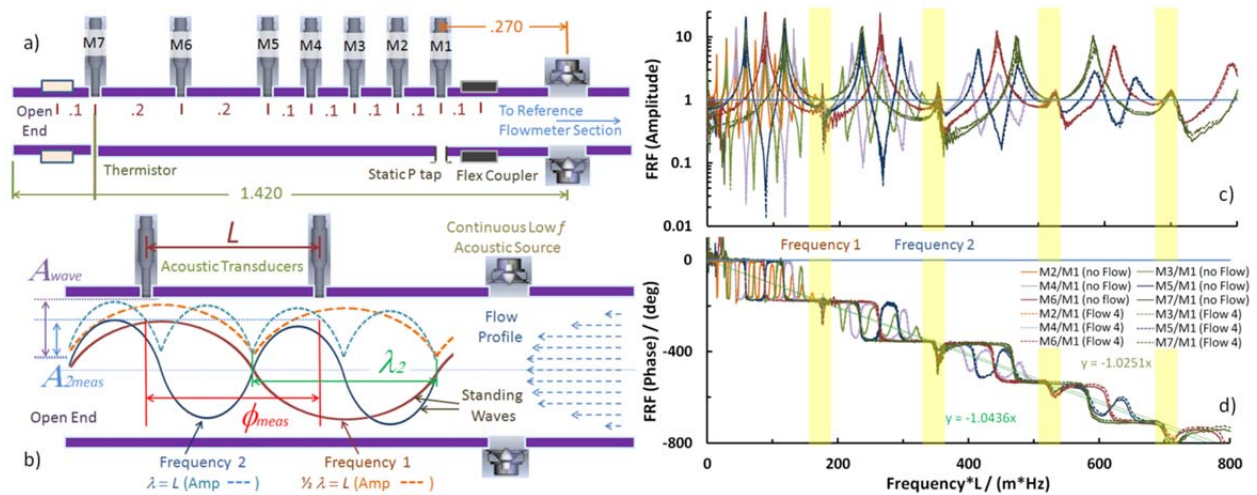

Figure 3: The broadband frequency-based LWAF concept. (3a) The LWAF geometry for time and frequency based measurements presented in this paper. (3b) An Illustration of standing waves generated by reflections from the open end and the parameters A, $\Delta\phi$ and λ that we measured. (3c/d) Amplitude and phase (respectively) of the frequency response function (FRF) between microphone pairs, each referenced to M1 and normalized on the x axis by the distance between microphones L. Plots with flow are indicated as dashed lines.

In specific cases, such as the waves shown with f_1 and f_2, the loudspeaker is tuned such that the wavelength of sound

$$\lambda_n = 2L/n \tag{4}$$

is equal to a multiple of ½ L. At these frequencies, LWAF response can be evaluated to obtain

$$c = 2f_n L/n \tag{5}$$

and

$$Ma = V/c = \Delta\phi_n/(n\pi) = \omega_n \Delta t/(n\pi) \tag{6}$$

where $\Delta\phi_n = \phi_{\text{flow}} - \phi_{\text{no flow}}$ and $\phi_{\text{no flow}} = \pi n$, where $\phi_{\text{no flow}}$ is measured in radians [3]. We refer to this approach as the "phase selection" method. It can be seen from Fig. 3b that microphone positioning relative to the open end of the duct is critical because the measured level, A_{meas} is only a fraction of A_{wave}, dependent upon where standing waves with λ_n align with where microphones are located. If A_{meas} is not large enough relative to the turbulence floor, it becomes difficult to obtain a reliable measurement. Effective microphone placement, which can be determined through optimization at a nominal c, allows for simultaneous measurement of many $A_{n\,meas}$ that are above the noise floor, at f_n below duct cut-on.

A frequency response function (FRF) is a comparison of acoustic pressure at two points in space, presented in Fig. 3 as a spectrum of amplitude $A = p_2/p_1$ (3c), and phase, $\phi = \phi_{m2} - \phi_{m1}$ (3d) as a function of normalized frequency (fL). This presentation is chosen because each data set is aligned by λ along x-axis, allowing λ_n to be located approximately (as highlighted). Within these bands, f_n can be determined using the FRF magnitude as the point where $A = 1$. Deviations from a linear frequency response result from the way that standing wave patterns align with microphone locations. Peaks and valleys correspond to a pressure node at the upstream and downstream microphones, respectively. A LWAF could measure c using the modal response of the duct and V could be obtained directly from the slope of the phase plot over a limited frequency range. Were an anechoic termination used, allowing only outgoing propagations, the FRF would become linear with f matching the blue $A = 1$ line and green interpolation lines in Figs. 3c and 3d.

These experiments use an amplified sine sweep source generated over a frequency range of 20 kHz to 2 kHz. Pressure is time averaged over a 20 s interval using ten, two-second time averages, resulting in a FRF bin width of 0.5 Hz. Comparing plots with and without flow, one can see that the FRF A is nearly identical due to the fact that λ is constant regardless of flow. There are noticeable changes near the peaks and valleys of the FRF which results from the fact that the standing wave generated by the LWAF has low amplitude relative to the flow-noise-level at one of the microphones. Values of c are obtained in the phase selection method by searching highlighted regions for f_n, where the FRF $A = 1$, *i.e.* where ½ λ multiples exist. Phase is evaluated at each of these frequencies and compared to $\phi_{\text{no flow}}$ to measure V. The 0.5 bin width of the FRF leads to a 0.03 % uncertainty in c. Spline interpolation is used to obtain better frequency resolution for obtaining f_n.

The seven microphones chosen for this LWAF configuration allow for four microphone pairs with $L = 0.1$ m spacing (M2/M1, M3/M2, M4/M3, M5/M4) to be simultaneously analyzed as shown in Figure 3a. In addition, we can analyze microphone pairs with $L = (0.2, 0.3, 0.4, 0.5, 0.6, 0.7$ and $0.8)$ m spacing. Each pair of microphones has a total of $n_{freq} = L/L_{min}$ (where L_{min} is 0.1 m, the minimum spacing) possible points on the FRF where $c + V$ can be evaluated using the phase selection method. We can therefore evaluate 72 possible data points with this setup. A subset of 21, (listed in Fig. 4c's legend) is chosen for simplicity, referenced to M1 whose relative position to other microphones can be found in Fig. 3a.

A second "slope method" determines V using the fact the linearly interpolated slope of the FRF phase averages the phase change with velocity across the FRF. This measurement obtains

$$c + V = \frac{2\pi L}{\partial \phi / \partial f} \tag{7}$$

.

One must determine c independently using either Eq. (5) with the aforementioned approach (as in data presented here) or by other means such as NIST's Reference Fluid Thermodynamic and Transport Properties Database (REFPROP) v9.0 [10], or by measuring wavelength at resonance and anti-resonance frequencies of the ducted geometry. Results from each of the two approaches are shown in Figure 4.
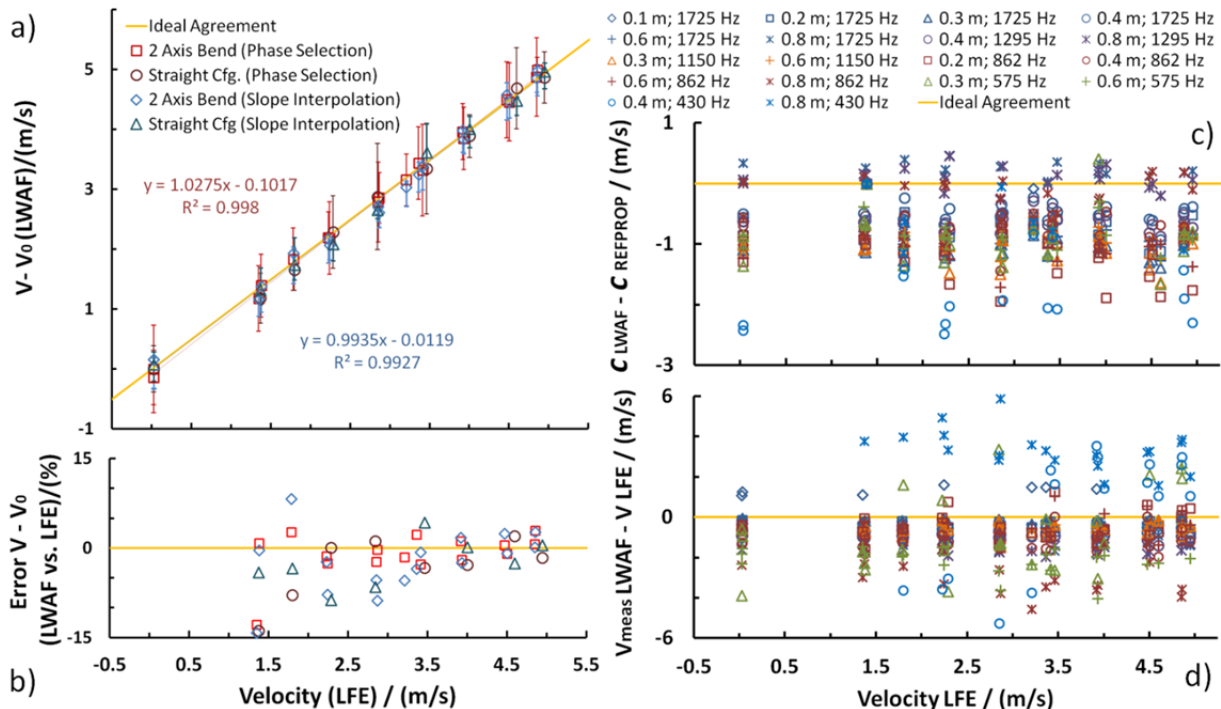

Figure 4: Experimental results from frequency based LWAF measurements. (4a/b) Present the correlation and error between measurements taken by the LWAF using both the slope interpolation and point frequency selection methods relative to the LFM. Error bars in (4a) correspond to the standard deviation of all readings taken. (4c/d) Show the variation of non-V_0-corrected individual measurements of c and V respectively to give a sense of error.

The data from the "slope" interpolation and "phase" selection methods are each aligned using the V_0 measurement result from each microphone pair. Data are plotted vs. the reference velocity measured by the LFM. The $k = 1$ uncertainty of these velocity measurements is 4.9 % and 4.3 %, over the full range of flows tested. If flows below 2 m/s are omitted from the analysis, the uncertainties decrease to 4.0 % and 1.9 %, respectively. The large error for low-flow measurements is caused by the difficulty in measuring small phase changes in a noisy signal. A higher statistical deviation is present in the slope interpolation method due to spectral noise in the FRF and our reporting of an average of a larger number of data points in the phase selection method. Uncertainties are of similar order for the straight and 2-axis bend cases tested with respective average errors by microphone pair of 0.58 m/s and 0.43 m/s for c and 0.35 m/s and 0.30 m/s for V. The similarity of these results is a good indication that the method is insensitive to the swirling flow, with the bend case performing slightly better in these experiments.

Figures 4c and 4d show the raw c and V measurements made by each of the microphone pair using the phase selection method. There is a clear bias in these data by microphone pair relative to the reference measurement. Average measurements of c and V are systematically low by 0.79 m/s (or 0.23 %), and 0.60 m/s respectively. Individual microphone pair measurements of V agree more closely with the zero flow condition measurement than they do the reference value. The average difference between each microphone pair and the reference improves from 1.7 m/s to 0.32 m/s if each microphone pair is normalized by the measured V_0.

As the bias is present in the no flow case, it may result from uncertainty in L (a nominal value is used from fabrication), systematic error in spline interpolation, leakage in the facility downstream of the LFM, and possible microphone calibration errors. Relative L correction will be used in future work, using long-time-averaged, no-flow measurements to account for differences. For the lab facility, distances will be calibrated by measuring propagations in a well characterized fluid such as argon. A higher resolution FFT will mitigate a need for interpolation. However, higher resolution means longer averages that do not allow transients in flow to be readily reported. The sweep signal used in these measurements was considered as a possible source of bias. Repeated measurements at varying sweep rates correlate well provided there is a high measured coherence across the frequency range used. Coherence is a statistical measurement of the correlation between two signals over a series of temporal averages.

Randomness in these data with respect to flow is lower in order, arising from turbulence noise in flow cases, variation in flow conditions over a measurement (LFM conditions are measured at the beginning and end of the data set and averaged) and vibration transmitted to the microphones. Compounded random uncertainties in our measurement devices also contribute to this result. Longer time series can be used to average the effects of turbulence. Reference measurements can be taken in parallel with LWAF data provided communication lag is not an issue between the cDAQ system and the CPU.

A small amount of bias may be introduced in Fig 4c due to our implementation of NIST's REFPROP as the c reference. We assumed that the ambient air, when dried, was a mixture of N_2, O_2, Ar, CO_2, and CH_4 with mole percentages (78.084, 20.946, 0.934, 0.0394, and 0.0002),

respectively [9]. We measured the humidity and reduced these mole percentages in proportion to account for the H_2O content. Probably, the actual composition varied during the measurements; however, these changes were too small to detect. The LFM has a calibrated 0.2 % uncertainty in volumetric flow, which is small relative to other observed errors. Error is introduced when the LFM measurement is converted to velocity through the LWAF as nominal PVC pipe. Manufacturer tolerance for diameter allows for variations that are as much as 2 % over length resulting in a possible 4 % bias in velocity between given microphone pairs. Temperature and pressure are only measured at one location in the LWAF, which increases uncertainty in the reported c and ρ.

4. Flow Measurement in the Time Domain

The performance of a time-of-flight based method of flow monitoring that tracks a series of pulses through the LWAF is evaluated in this section as described in Fig. 5. Unlike the standing-wave approach, reflected waves are not reinforced by a continuously driven loudspeaker. Instead, a traveling pressure wave packet is generated using a pulsed source. These packets dissipate by radiation from the duct's open end and through absorption by the walls of the duct. The wave packet can be tracked at multiple axial locations to determine its propagation speed, as shown in Fig. 5a. For a no-flow case, the packet travels at the speed of sound c and when flow is present, the wave packet travels at $c + V$ downstream and $c - V$ upstream.
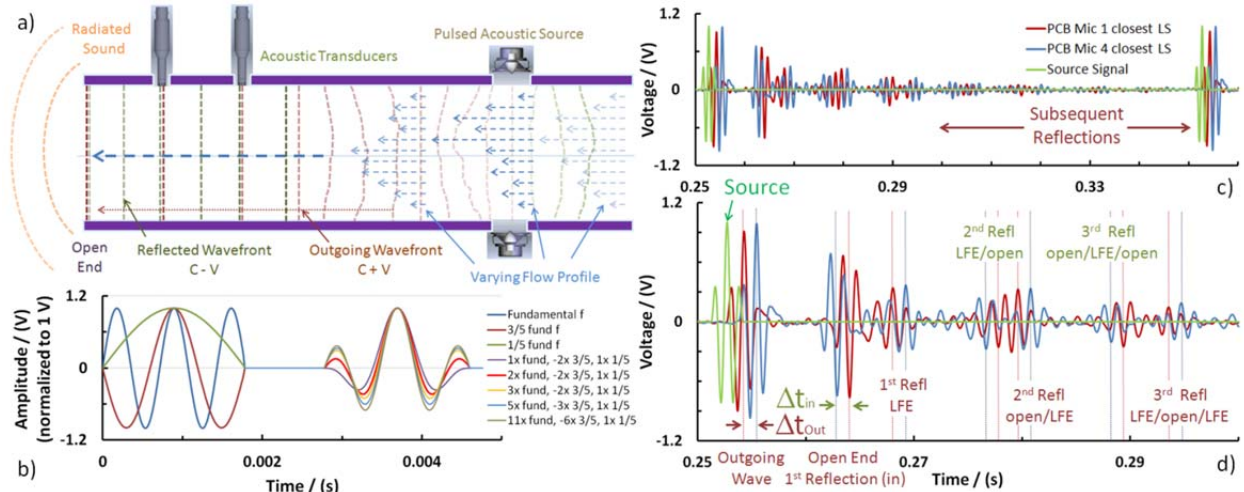

Figure 5: The mechanics of the time based LWAF. (5a) Illustrates how traveling pulses propagate through a long wavelength flowmeter (wavefront lightness representing passage of time). (5b) The construction of a pulsed signal that contains exclusively low frequency signals. (5c/d) Time plots showing reflections measured by two adjacent microphones under zero flow conditions (red = time delay of outgoing pressure waves, green = time delay of incoming pressure waves).

The 7 axially spaced microphones from Fig. 3a were used to track a series of pulses of sound through the LWAF. The parameters c and V were calculated using

$$c = \frac{L}{\Delta t_{avg}} = \frac{2L}{\Delta t_{out} + \Delta t_{in}} \tag{8}$$

$$V = \frac{L}{\Delta t_{avg} - \Delta t_{out}}, \qquad (9)$$

where   and   are the measured times it takes for the disturbance to propagate the distance L as shown in Fig. 5d. Additional peaks can be tracked similarly providing additional data from a single pulse; for simplicity, we measured only a single outgoing and incoming wavefront.

The signal used in these studies is generated using only the low-frequency information as illustrated in Fig. 5b. This feature ensures that the wave packet propagates as a plane wave rather than as a higher order mode where cross propagation slows axial velocity. One and a half periods of a sine wave with $f = f_0$ (a fundamental f below cut-on) are summed with an inverted $3/5\ f_0 = f_1$ and $1/5\ f_0 = f_2$, wave, each with an amplitude that accentuates the central peak as shown to the right. A simple summation of, $f_0 - f_1 + \frac{1}{2}f_1$ is chosen for measurements presented here as shown in red. The microphone response is monitored at 51.6 kHz. A total of 11 points around the peak frequency are fit with a polynomial to resolve the time when the measured maximum of the pulse occurs.

Results from the time based LWAF shown in Figure 6 agree with the LFM to a standard deviation of (5.3, 2.1, 2.8, 1.4 and 2.7) % for increasing f_0 signals of (0.8, 1.2, 1.4, 1.6 and 2.0) kHz respectively.
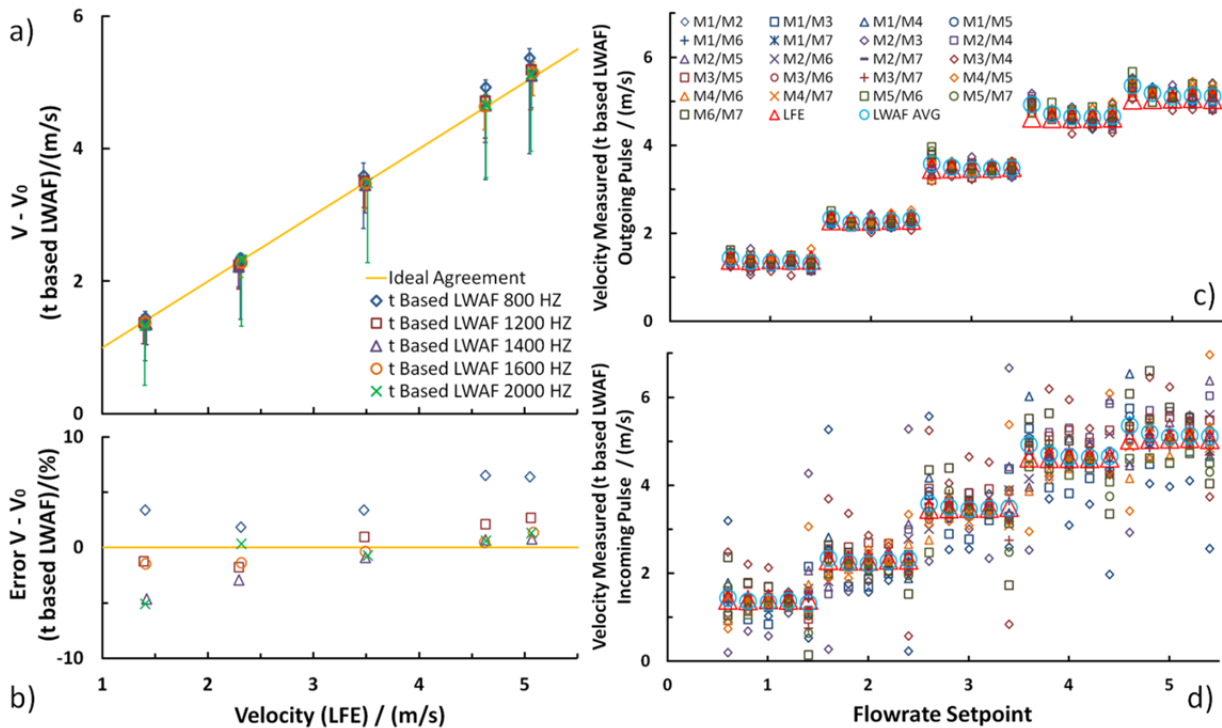

Figure 6: Experimental results of the time based LWAF approach. (6a/b) Correlation and error between LWAF measurements ($f_0 =$ (0.8, 1.2, 1.4, 1.6, and 2.0) kHz) vs. LFM. The positive and negative error bars in (6a) correspond to the standard deviation between outgoing and incoming wavefront measurements respectively, by each

microphone pair. (6c/d) Averaged LFM, LWAF and individual microphone pair measurements vs. flow cases (#'s correspond to Table 1, Col. B). Results at a given flow are separated by f_0, from least to greatest.

Figures 6c and 6d illustrate a significantly higher deviation of reflected sound measurements returning from the duct's open end. Average individual microphone pair deviations of (6.9, 4.1, 3.9, 3.8 and 4.9) % for outgoing and (26.6, 12.9, 12.1, 7.4 and 32.3) % are observed. This is expected due to the lower signal-to-noise ratio for the incoming wave measurement, which is particularly evident for higher f_0 cases, where the reflection coefficient is lower. The lower f_0 cases also have higher deviation due to the fact that finding the exact peak becomes less precise as the peak is broadened in time. The best tested time based flowmeter uses a f_0 of 1.6 kHz resulting in a measurement standard deviation of 1.4 % for averaged LWAF results relative to the LFM.

Similar sources of error exist for a time-of-flight based approach as discussed for the FRF based method.   In addition, a significant dependence of $c + V$ on f_0 has been observed which is dissimilar for measurements of outgoing and incoming waves.   We do not understand this phenomenon at present; however, the deviations for each microphone pair can be removed by calibration using data from no-flow measurements and a known speed of sound (as determined by REFPROP or as measured in a no-flow situation conditions). Pulses in these experiments are repeated at 0.15 s intervals to allow time for reflections to dissipate. Data were taken during 9 minutes with a total of 1790 measured outgoing and incoming pulses. The average standard deviation of $c + V$ over time for each microphone pair was 0.1 % and was as high as 0.5 % for smaller L.

The time based method has uncertainty resulting from the curve fitting algorithm used to find the maximum peak location. This algorithm performs significantly better than simply selecting the highest measured point. The discretized time step of measured waveforms is 0.0194 ms, which correlates to a $c + V$ difference of 6.6 % and a V difference of 1750 % for the $L = .1$ m, $V = 1.3$ m/s case. Our results show that by using a curve fitting approach, discretization uncertainty is reduced significantly. If sampling frequency were increased, the meter's overall uncertainty would be improved, and results would rely less heavily on this interpolation.

5. **Conclusions and Discussion**

Frequency based measurements have a standard deviation of 4.9 % and 4.3 % using data point selection and the slope of the FRF to determine V. The best time based approach has a 1.4 % standard deviation using a 1.6 kHz pulsed signal. Measurements reported are preliminary and indicate progress towards the project's goal of 1 % measurement uncertainty over flows of (0 to 30) m/s. Further refinement of our experimental approach and data analysis will reduce uncertainty for each flowmeter concept.

Now that techniques have been validated for the 1:100 scale facility in low flows, we will integrate a larger scale blower to increase maximum velocity to 32 m/s. We will evaluate other facility configurations including cases with T-junctions, turbulence generators, and cases with increased swirl and other obstruction introduced flow distortions to quantify the robustness of our techniques. A LWAF measurement setup is scheduled to be implemented on two new

facilities at NIST, using the Building and Fire Research Lab's new exhaust stack and the Fluid Metrology Group's large duct flow simulation facility currently being calibrated by the Colorado Experiment Engineering Station Inc. (CEESI). Using these facilities, methods will be stressed in a similar flow environment to a power plant stack. Ultimately, refined techniques will be evaluated at a full scale power plant and this work will hopefully lead to a lower cost, lower uncertainty alternative for measuring power plant exhaust flows.

6. **Acknowledgements**

References:

[1] Robertson, B., *Effect of Arbitrary Temperature and Flow Profiles on the Speed of Sound in a Pipe*, J. Acoust. Soc. Am., Vol. 62, No. 4, pp. 813-818 (1977).

[2] Potzick, J. E., Robertson B., *Long-Wave Acoustic Flowmeter*, ISA Transactions, Vol 22, No. 3, pp. 9-15, (1983).

[3] Potzick, J. E., Robertson, B., *Long Wavelength Acoustic Flowmeter*, United States Patent 4,445,389. (1984).

[4] Lighthill, M. J., *On Sound Generated Aerodynamically. I General Theory*, Proc. R. Soc. Lond. A 20 vol. 211 no. 1108, pp. 564-587, (1952).

[5] *Composites for Clean Coal Energy*, AOC Resins, Case Study (2008).

[6] Anderson, D. K., Maroti, L. A., *Designing Wet Duct/Stack Systems for Coal-Fired Power Plants*, Power Magazine, March, 15 (2006).

[7] Wright, J. D., Johnson, A. N., *NIST Lowers Gas Flow Uncertainties to 0.025% or Less*, NCSL International Measure, Vol. 5, pp. 30-39, (2010).

[8] In order to describe materials and experimental procedures adequately, it is occasionally necessary to identify commercial products by the manufacturer's name or label. In no instance does such identification imply endorsement by the National Institute of Standards and Technology, nor does it imply that the particular product or equipment is necessarily the best available for the purpose.

[9] Reduced from NOAA Earth System Research Laboratory (2012) *data obtained via Wikipedia.*

[10] Lemmon, E. W., Huber, M. L., and McLinden, M. O., *NIST Standard Reference Data Base 23: Reference Fluid Thermodynamic and Transport Properties,Version 9.0*, National Institute for Standards and Technology, Standard Reference Data Program, Gaithersburg, MD, (2010).